# Pulse-energy dynamics of passively mode-locked solid-state lasers above the *Q*-switching threshold

**Adrian Schlatter, S. C. Zeller, R. Grange, R. Paschotta, and U. Keller**

*Institute of Quantum Electronics, Physics Department, Swiss Federal Institute of Technology (ETH), ETH Zürich Hönggerberg, Wolfgang-Pauli-Strasse 16, 8093 Zürich, Switzerland*

Received August 26, 2003; revised manuscript received February 27, 2004; accepted April 1, 2004

We have investigated the dynamical behavior of various passively mode-locked solid-state lasers by measuring how a modulation of the pump power affects the output power. We show theoretically and experimentally how the damping of the relaxation oscillations is reduced and finally becomes zero when the pump power is reduced so that the threshold for *Q*-switched mode locking is approached. For the first time to our knowledge, this method provides important information on the stability of mode locking above the *Q*-switched mode-locking threshold. It is applicable to lasers that are mode locked with slow-saturable absorbers. The results helped to explain the cause of unexpectedly low *Q*-switching thresholds in two cases. Also we obtain some useful spectroscopic information. © 2004 Optical Society of America

*OCIS codes:* 140.3580, 140.4050, 140.3540.

## 1. INTRODUCTION

Passively mode-locked solid-state lasers have become pulse sources for a great variety of applications.[1] In most cases, stable mode locking with constant pulse energy is the desired regime of operation. However, the passive mode-locking element, e.g., a semiconductor saturable-absorber mirror[2,3] (SESAM), usually introduces a tendency for *Q*-switching instabilities.[4–6] This has been a problem in passively mode-locked solid-state lasers for more than 25 years.[1] Reliable self-starting and stable mode locking has been demonstrated with SESAMs for the first time in 1992[2] and applied to many different laser materials and cavity designs since then.

Typically, one observes the *Q*-switched mode-locked (QML) regime for pump powers below a certain threshold value. In this regime, the pulse energy is not stable but oscillates in a wide range. For some design goals, in particular for very high pulse-repetition rates in the multi-GHz regime, it is a challenge to find designs for which the QML threshold can be exceeded so as to obtain stable mode locking. It is therefore of great interest to develop a detailed quantitative understanding of the pulse-energy dynamics.

So far, intensive investigations have addressed the factors that determine the QML threshold itself. However, more recently with Er:Yb:glass lasers (Refs. 7–10), we observed considerably lower QML threshold values than predicted in Ref. 6. The following investigations resolved this mystery at least for a 61-MHz Er:Yb:glass laser, and the same explanation probably also holds for the higher pulse-repetition rates.

In this paper, we investigate the dynamics of various passively mode-locked solid-state lasers above the QML threshold. Our method is to apply a small modulation with variable frequency to the pump power and to monitor the corresponding modulation of the average output power of the mode-locked laser. The relation between pump and output modulation defines the frequency-dependent transfer function. From this function, we can determine the frequency and the damping of the relaxation oscillations. *Q*-switching instabilities can be interpreted as the occurrence of undamped relaxation oscillations. We show experimentally that the damping of the relaxation oscillations approaches zero as the pump power is decreased toward the QML threshold. By comparing the damping with theoretically expected values, we can verify the understanding of the dynamics in the regime above the QML threshold. We also compare the dynamics with and without the SESAM in the cavity in order to demonstrate its influence on the relaxation oscillations.

In simple cases, the new method produced results that are in agreement with theoretical expectations. In other cases, where the QML threshold deviates from the expected value, our measurements lead to explanations for these effects. We demonstrate that useful data on SESAMs can be produced, including cases where the direct measurement of SESAM parameters would be very difficult. As a side product, we obtained some useful spectroscopic information on the energy transfer in Er:Yb-doped glass.

In Section 2, we describe the theoretical derivation of the transfer function. Experimental results for various lasers are presented in Section 3. Finally we draw some conclusions in Section 4.

## 2. THEORY

### A. Differential Equations

We first describe the behavior of a three-level laser system and then explain the changes (i.e., simplifications)

needed for a four-level system. The dynamics of such a laser are described by two coupled differential equations:

$$\frac{\mathrm{d}P}{\mathrm{d}t} = \frac{g - l - q_\mathrm{P}(E_\mathrm{P})}{T_\mathrm{R}} P, \tag{1}$$

$$\frac{\mathrm{d}g}{\mathrm{d}t} = \frac{g_0 - g}{\tau_\mathrm{L}} + \frac{\eta(g) P_\mathrm{P}}{E_\mathrm{sat,L}} - \frac{P}{E_\mathrm{sat,L}} g, \tag{2}$$

where $P$ is the intracavity average laser power, $g$ is the power gain per round trip, $T_\mathrm{R}$ is the cavity roundtrip time, $l$ are the linear losses, $q_\mathrm{P}(E_\mathrm{P})$ describes the nonlinear losses at the saturable absorber, $E_\mathrm{P} = P \times T_\mathrm{R}$ is the pulse energy, $g_0$ is the gain in the unpumped crystal ($<0$ for three-level lasers), $\tau_\mathrm{L}$ is the upper-state lifetime, and $E_\mathrm{sat,L} = A_\mathrm{L} h\nu_\mathrm{L}/(m\sigma_\mathrm{tot})$ is the gain saturation energy, where $A_\mathrm{L}$ is the effective laser mode area in the crystal, $h\nu_\mathrm{L}$ is the energy difference of the laser levels, $m$ is the number of passes through the gain medium per round trip (typically two for a linear cavity), and $\sigma_\mathrm{tot} = \sigma_\mathrm{em} + \sigma_\mathrm{abs}$ is the sum of the emission and the reabsorption cross section at the laser wavelength. $P_\mathrm{P}$ is the pump power, and $\eta(g)$ is the pump efficiency (including absorption efficiency and quantum defect). The absorption efficiency depends on the population of the lower pump level and therefore on $g$. Using a simple model for a slow-saturable absorber (pulse length $\tau_\mathrm{P}$ is much shorter than the absorber recovery time $\tau_\mathrm{A}$) that fully recovers within a round-trip time ($\tau_\mathrm{A} \ll T_\mathrm{R}$), we have

$$q_\mathrm{P}(E_\mathrm{P}) = \frac{\Delta R}{S}[1 - \exp(-S)], \quad S = \frac{E_\mathrm{P}}{E_\mathrm{sat,A}}. \tag{3}$$

Here, $\Delta R$ is the modulation depth (maximum reflectivity change) of the saturable absorber, and $E_\mathrm{sat,A} = A_\mathrm{A} \times F_\mathrm{sat,A}$ is the saturation energy given as the product of the effective mode area on the absorber and the saturation fluence of the absorber.

The cw laser (with the SESAM replaced by a highly reflecting mirror) is described by the same differential equations, but with $q_\mathrm{P}(E_\mathrm{P}) \equiv 0$ and possibly with a somewhat smaller value of $l$.

In the case of a four-level laser, there is no reabsorption loss in the crystal. Therefore we have $g_0 = 0$ and $\sigma_\mathrm{tot} = \sigma_\mathrm{em}$. Additionally, the absorption efficiency is typically only weakly dependent on the gain. Typically, it may be approximated to be 1.

### B. Transfer Function

In order to find the transfer function, we linearize the differential equations (1) and (2) around the steady state and also allow the pump power to vary. Defining $\delta P = P(t) - P$, $\delta g = g(t) - g$, and $\delta P_\mathrm{P} = P_\mathrm{P}(t) - P_\mathrm{P}$, where $P, g$, and $P_\mathrm{P}$ denote the steady-state values, we find

$$\frac{\mathrm{d}}{\mathrm{d}t}\begin{pmatrix}\delta P \\ \delta g\end{pmatrix} = \begin{bmatrix}\alpha & \beta \\ -\gamma & -\epsilon\end{bmatrix}\begin{pmatrix}\delta P \\ \delta g\end{pmatrix} + \zeta\begin{pmatrix}0 \\ \delta P_\mathrm{P}\end{pmatrix}, \tag{4}$$

where

$$\alpha = -P\frac{\partial q_\mathrm{P}}{\partial E_\mathrm{P}}(E_\mathrm{P}), \quad \beta = \frac{P}{T_\mathrm{R}}, \quad \gamma = \frac{g}{E_\mathrm{sat,L}},$$

$$\epsilon = \frac{1}{\tau_\mathrm{L}} + \frac{P}{E_\mathrm{sat,L}} + \frac{P_\mathrm{P}}{E_\mathrm{sat,L}}\frac{\partial \eta}{\partial g}(g), \quad \zeta = \frac{\eta(g)}{E_\mathrm{sat,L}}.$$

If we set $\delta P_\mathrm{P} = 0$ for a moment, we find the criterion for stable mode locking[5,6] (QML criterion) by requiring that the eigenvalues have negative real parts. This leads to the condition $\epsilon > \alpha$. In this regime, we have damped relaxation oscillations with the frequency

$$f_\mathrm{ro} = \frac{1}{2\pi}\left[\beta\gamma - \alpha\epsilon - \frac{1}{4}(\epsilon - \alpha)^2\right]^{1/2} \tag{5}$$

and the damping time

$$\tau_\mathrm{ro} = \frac{2}{\epsilon - \alpha}.$$

(We have assumed to have typical parameters of solid-state lasers, where the radicand in Eq. (5) is positive.)

For $\epsilon < \alpha$, initially small deviations from the steady state will rapidly grow, so that the linearized equations are no more applicable. This is the regime of Q-switched mode locking.

In the stable regime, we define the transfer function $\chi(\omega)$ as the ratio of the complex amplitudes of the oscillation of output power and pump power, when a harmonic modulation is applied to the pump power according to $\delta P_\mathrm{P} = B\sin(\omega t)$. By solving the differential equations, we find

$$\chi(\omega) := \frac{\delta P_\mathrm{out}}{\delta P_\mathrm{P}} = \frac{T_\mathrm{oc}\beta\zeta}{-\omega^2 + (\epsilon - \alpha)i\omega + \beta\gamma - \alpha\epsilon}. \tag{6}$$

### C. Properties of the Transfer Function

Analyzing the modulus of the transfer function (Fig. 1), we identify the following characteristic parameters. The resonance frequency (frequency of the peak) is

$$f_\mathrm{res} = \frac{1}{2\pi}\left[\beta\gamma - \alpha\epsilon - \frac{1}{2}(\epsilon - \alpha)^2\right]^{1/2}. \tag{7}$$

The parameter

$$\begin{aligned}\xi &\equiv {f_{1/2}}^2 - {f_\mathrm{res}}^2 \\ &= \frac{\sqrt{3}}{4\pi^2}(\epsilon - \alpha)\left[\beta\gamma - \alpha\epsilon - \frac{1}{4}(\epsilon - \alpha)^2\right]^{1/2} \\ &= \frac{\sqrt{3}}{\pi}\frac{f_\mathrm{ro}}{\tau_\mathrm{ro}}\end{aligned} \tag{8}$$

characterizes the width of the resonance peak. Here, $f_{1/2}$ is the (higher) frequency, where the modulus of the transfer function has fallen to half its peak value. We use this type of width parameter (instead of, e.g., the full width at half-maximum) because the parameter $\xi$ is directly related to the damping time $\tau_\mathrm{ro}$ of the relaxation oscillations.

The peak height of the modulus of the transfer function is

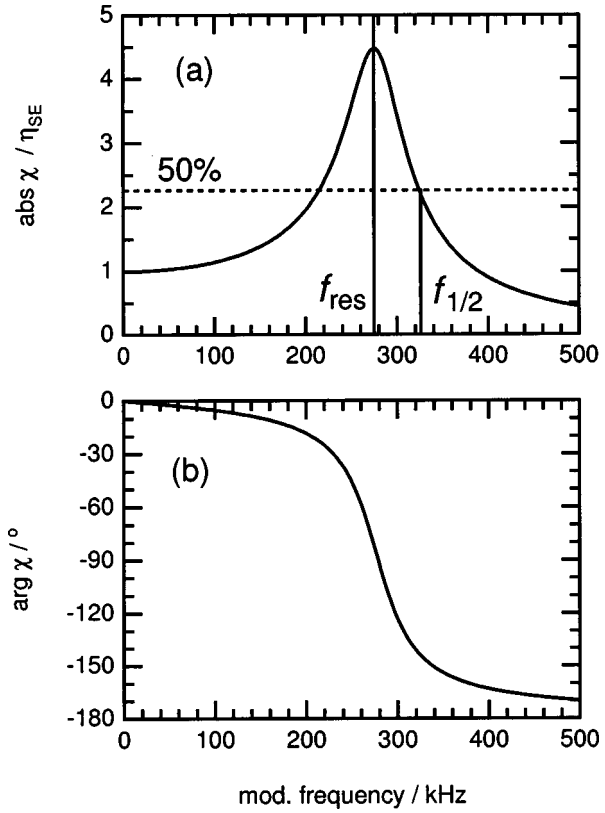


Fig. 1. (a) Modulus and (b) phase of a typical transfer function. The transfer function is completely characterized by the resonance frequency (frequency where the modulus of the transfer function has a peak), the peak width, and the peak height.

$$\hat{\chi} = \frac{1}{2\pi} \frac{T_{oc}\beta\zeta}{(\epsilon - \alpha)\left[\beta\gamma - \alpha\epsilon - \frac{1}{4}(\epsilon - \alpha)^2\right]^{1/2}} = \frac{1}{4\pi} T_{oc}\beta\zeta \frac{\tau_{ro}}{f_{ro}}.$$

Using these parameters, we can rewrite the modulus and phase of the transfer function, which we now interpret as a function of the frequency $f$ instead of the angular frequency $\omega$:

$$|\chi(f)| = \frac{\hat{\chi}\xi}{\left[3\left(f^4 - 2f_{res}{}^2 f^2 + \frac{1}{3}\xi^2 + f_{res}{}^4\right)\right]^{1/2}}, \quad (9)$$

$$\arg\chi(f) = -\arctan\frac{f\left\{2\left[\left(f_{res}{}^4 + \frac{1}{3}\xi^2\right)^{1/2} - f_{res}{}^2\right]\right\}^{1/2}}{\left(f_{res}{}^4 + \frac{1}{3}\xi^2\right)^{1/2} - f^2}. \quad (10)$$

For $f = 0$, the transfer function must equal the slope efficiency.

Typically we have $\epsilon^2 \ll \beta\gamma$. In this case, the resonance frequency $f_{res}$ can be approximated as

$$f_{res} \cong \frac{1}{2\pi}\sqrt{\beta\gamma} = \frac{1}{2\pi}\left(\frac{Pg}{T_R E_{sat,L}}\right)^{1/2}. \quad (11)$$

It follows that

$$f_{ro} \cong f_{res},$$

and we also have

$$\tau_{ro} = \frac{\sqrt{3}}{\pi}\frac{f_{ro}}{\xi} \cong \frac{\sqrt{3}}{\pi}\frac{f_{res}}{\xi}.$$

## 3. EXPERIMENTAL RESULTS

We have measured the transfer functions of four lasers, differing in gain material, wavelength, and pulse-repetition rate.

### A. Nd:$YVO_4$ Laser at 1064 nm

Nd:$YVO_4$ is a popular gain medium that has been frequently used in SESAM mode-locked lasers, including lasers with high average output powers of up to 20 W (Ref. 11) and with high pulse-repetition rates as high as 157 GHz (Ref. 12). For our investigations, we started with a Nd:$YVO_4$ laser of moderate power and repetition rate. The $Q$-switched mode-locking threshold of this laser and the SESAM parameters had been characterized carefully and had been found to be consistent with theoretical calculations. The geometry of the laser cavity is shown in

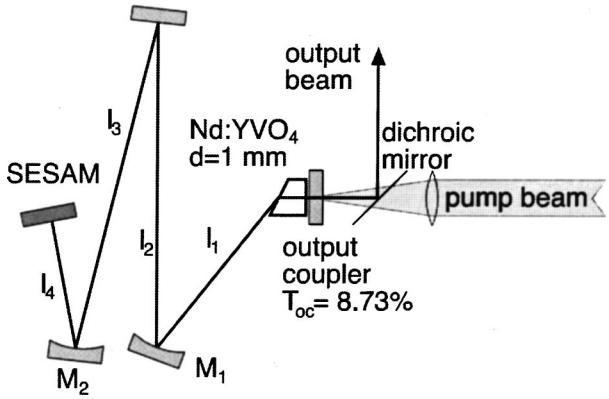


Fig. 2. Nd:$YVO_4$ laser cavity. The beam radius in the crystal is designed to be 80 $\mu$m; the beam radius on the SESAM is 140 $\mu$m.

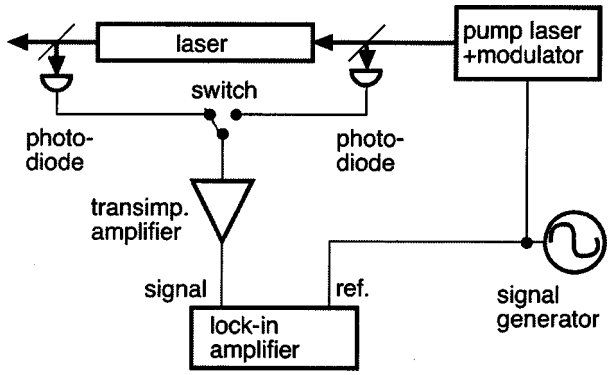


Fig. 3. Setup used for transfer-function measurements.

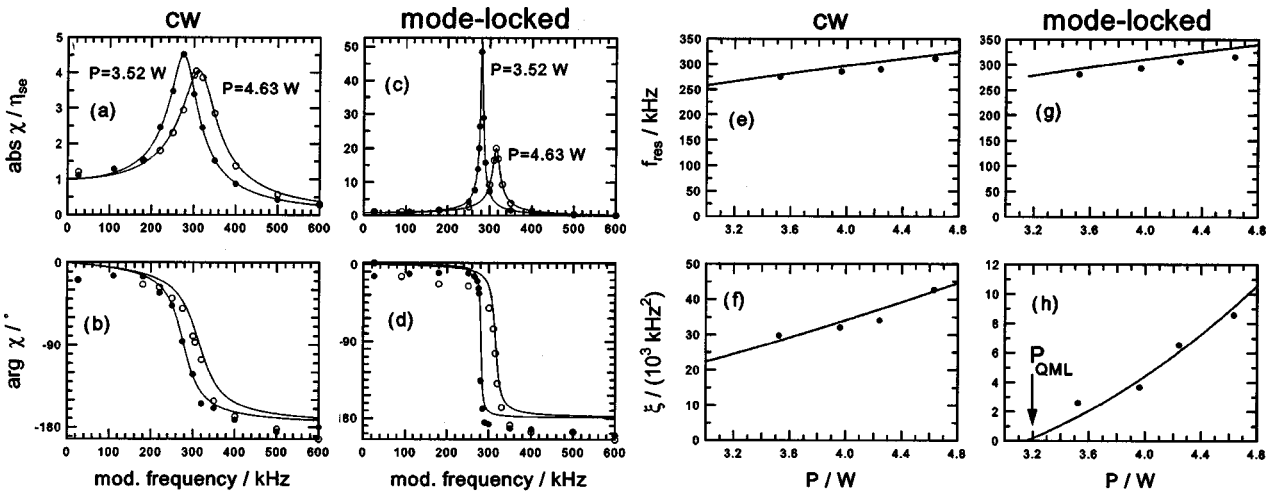


Fig. 4. (a), (b) Transfer functions of the cw and (c), (d) the mode-locked Nd:$YVO_4$ laser at the highest and lowest measured intracavity power. For clarity, the other curves are not shown here. (e)–(h) Parameters $f_{\mathrm{res}}$ and $\xi$ as functions of the intracavity power for the cw and the mode-locked laser.

Fig. 2. The laser is diode pumped at $\lambda_P = 808$ nm through the output-coupling mirror. A dichroic mirror is used to separate the output laser beam from the pump beam. The crystal has a Brewster interface to avoid reflection losses. Nd:$YVO_4$ has an emission cross section of $\sigma_{\mathrm{em}} = 114 \times 10^{-20}$ cm$^2$ at 1064 nm (Ref. 13). The used crystal is 1% neodymium doped and has an upper-state lifetime $\tau_L = 90\ \mu$s (Ref. 13). The mode locking is achieved with a SESAM with the following measured parameters: saturation fluence $F_{\mathrm{sat,A}} = 60\ \mu$J/cm$^2$, modulation depth (maximum reflectivity change) $\Delta R = 1.7\%$, nonsaturable losses $\Delta R_{\mathrm{ns}} = 1.3\%$, and recovery time $\tau_A = 26$ ps.

The laser generates 10.6-ps pulses at a repetition rate of 100 MHz. The average output power is up to 400 mW, and the QML threshold power (minimum output power for stable mode locking) was measured to be 280 mW. The relaxation oscillation frequency is ~300 kHz for maximum output power, in good agreement with the calculated value (Eq. 11).

### 1. Experimental Setup for Measurement of the Transfer Function

To measure the transfer function of the laser, we sinusoidally modulate the current of the pump laser diode and measure the amplitude and phase of the resulting modulation of pump and output power for a range of modulation frequencies. The setup is shown in Fig. 3. It consists of the pump laser and means to modulate its power. The amplitude and frequency of the modulation are controlled by a signal generator. The amplitude has to be chosen small enough to stay within the validity range of the linearized equations (4). Pump and output power are measured with silicon photodiodes and a transimpedance amplifier. A lock-in amplifier measures amplitude and phase of the modulation on the signal. The signal source can be manually switched between pump and laser output. The resulting function was scaled not by an absolute calibration of the amplified signal to the powers, but by requiring that the low-frequency limit must be identical to the slope efficiency $\eta_{\mathrm{SE}}$.

### 2. Results

The transfer functions of the mode-locked and the cw laser (where the SESAM is replaced with a highly reflecting mirror) were measured at four different intracavity power levels. We just show the transfer functions at the lowest and the highest measured intracavity power [Figs. 4(a)–4(d)]. The modulus of the measured transfer functions was fitted with the function given in Eq. (9), using $f_{\mathrm{res}}$, $\xi$, and $\hat{\chi}$ as fit parameters. The measured data as well as the fitted functions were afterwards scaled to meet $|\chi(0)| = \eta_{\mathrm{SE}}$. The phase data allow us to verify the obtained values of $f_{\mathrm{res}}$ and $\xi$ ($\hat{\chi}$ has no influence on the phase). The lines in the phase plots show the function given in Eq. (10) using the parameters from the above-mentioned fitting procedure, rather than doing another fit.

We have repeated the above-described measurement and fitting procedure for different intracavity power levels. The data can be nicely fitted in all cases. The calculated phase functions also agree with the measurement.

Figures 4(e)–4(h) show the fit parameters $f_{\mathrm{res}}$ and $\xi$ as functions of the intracavity power for the cw and the mode-locked laser. The measured QML threshold has been used as the first data point in the plot of the measured function $\xi(P)$ [namely, as $\xi(P_{\mathrm{QML}}) = 0$] and is marked by an arrow in Fig. 4(h). The curves in Figs. 4(e)–4(h) show the expected values [Eqs. (7) and (8)] calculated from the laser properties. The mode radii, the linear losses, and the SESAM parameters were chosen within their tolerances to achieve the best agreement. The used values are $l = 9\%$, $w_L = 62\ \mu$m, $\Delta R = 1.33\%$, $F_{\mathrm{sat,A}} = 60\ \mu$J/cm$^2$, $\Delta R_{\mathrm{ns}} = 1.0\%$, and $w_A = 140\ \mu$m.

In conclusion, the dynamic behavior of this laser is as expected from the theory. Compared with the cw laser, the passively mode-locked laser exhibits a weaker damping of the relaxation oscillations, because the SESAM introduces a lower loss for higher pulse energies. If we reduce the pump power, we approach a critical point where

the damping becomes zero. Below this point, fluctuations of the pulse energy grow exponentially and lead the laser into the $Q$-switched mode-locked regime.

### B. Nd:YLF Laser at 1321 nm

Nd:YLF lasers have been passively mode locked with SESAMs as early as in 1992 at 1.047 $\mu$m (Ref. 2) and in 1996 at 1.3 $\mu$m (Ref. 14). Here we investigated the dynamics of a 1321-nm laser of this kind. The QML threshold of this laser had been characterized earlier and was found to be unusually low compared with an estimate based on typical SESAM parameters. The actual SESAM parameters were unknown for lack of a measurement setup operating in the 1.3-$\mu$m region.

Figure 5 shows the laser cavity. The Brewster-angled Nd:YLF crystal is pumped with a Ti:sapphire laser at $\lambda_P = 797$ nm through one of the folding mirrors. The emission cross section was measured to be $\sigma_{em} = 2.0 \times 10^{-20}$ cm$^2$ at $\lambda_L = 1321$ nm. The upper-state lifetime is $\tau_L = 500$ $\mu$s (Ref. 15). The laser crystal has a neodymium doping of 1.2%. Passive mode locking is achieved with a SESAM.

The laser generates 48-ps pulses at a repetition rate of 119 MHz. The average output power is up to 630 mW (hardly less than with a highly reflecting mirror instead of the SESAM), and the QML threshold power is 55 mW. The relaxation oscillation frequency is ~80 kHz at maximum output power.

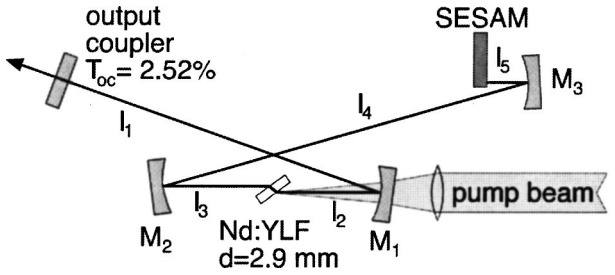


Fig. 5. Nd:YLF laser cavity. The beam radii in the crystal are designed to be 45 $\mu$m and 67 $\mu$m, in sagittal and horizontal direction, respectively, while the beam radius on the SESAM is 90 $\mu$m.

#### 1. Experimental Setup for Measurement of the Transfer Function

The setup is very similar to the one used for the Nd:$YVO_4$ laser (Subsection 3.A.1). Therefore we just mention the differences from that setup. Because the Nd:YLF laser is pumped by a Ti:sapphire laser, the pump power cannot easily be modulated electrically. Instead, an acousto-optic modulator has been inserted into the pump beam. Pump and output power are measured with a silicon and an InGaAs photodiode, respectively. A lock-in amplifier measures the voltage drop across a 50-$\Omega$ resistor.

#### 2. Results

The transfer functions of the mode-locked and the cw laser were measured at four different intracavity powers [Figs. 6(a)–6(d)]. The solid curves show the functions given in Eqs. (9) and (10) and were derived from the measured data in the same way as described above for the Nd:$YVO_4$ laser. Generally, it is possible to find $f_{res}$, $\xi$, and $\hat{\chi}$ so that the corresponding transfer function fits the data well.

The parameters $f_{res}$ and $\xi$ derived from the fits are shown in Figs. 6(e)–6(h) as functions of the intracavity power for the cw and the mode-locked laser. The curves show the calculated values [Eqs. (7) and (8)] using $l = 2.6\%$, $w_L = 47$ $\mu$m, $\Delta R = 0.02\%$, $F_{sat,A} = 20$ $\mu$J/cm$^2$, $\Delta R_{ns} = 0.8\%$, and $w_A = 90$ $\mu$m. The linear loss and the mode radii were varied within their tolerances for best agreement, whereas the SESAM parameters were chosen freely because we had no measured values to start from. Please note that, within the power range of the measurements, $f_{res}$ and $\xi$ strongly depend only on the product $\Delta R \times E_{sat,A} = \Delta R \times A_A \times F_{sat,A}$ but not on the individual values of $\Delta R$, $A_A$, and $F_{sat,A}$. This holds for sufficiently high SESAM saturation ($S$ parameter) where the exponential term in Eq. (3) can be neglected. The SESAM parameters needed to explain the frequency and damping of the relaxation oscillations are very low. To verify this result, we have estimated $\Delta R$ from the pulse length. We used

$$\tau_P \approx \frac{1.1}{\Delta f_g}\sqrt{\frac{g}{\Delta R}},$$

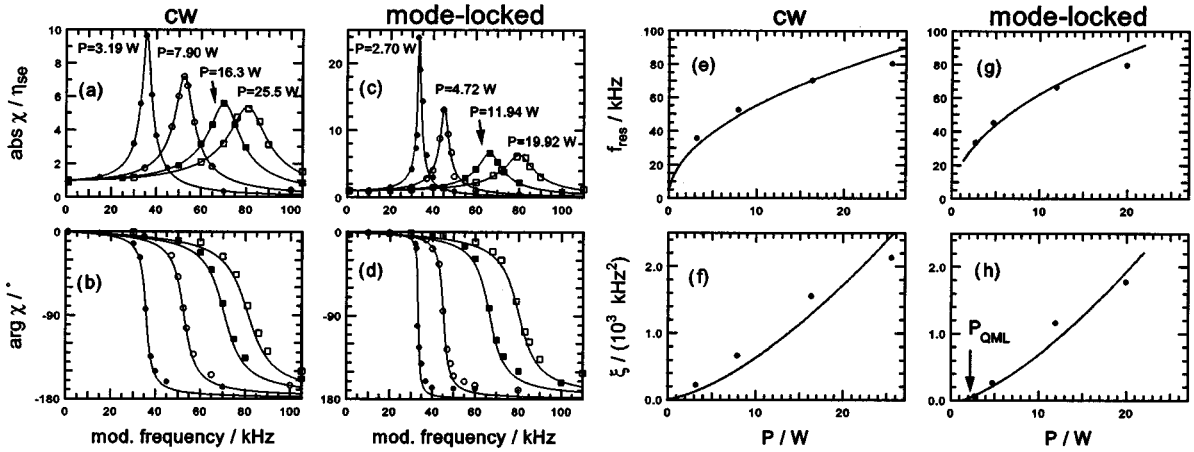


Fig. 6. (a), (b) Transfer functions of the cw and (c), (d) the mode-locked Nd:YLF laser. (e)–(h) Parameters $f_{res}$ and $\xi$ as functions of the intracavity power for the cw and the mode-locked laser.

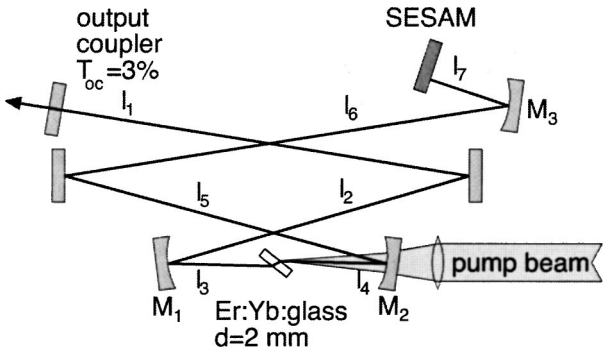


Fig. 7. 61-MHz Er:Yb:glass laser cavity. The sagittal and the tangential beam radius in the crystal are calculated to be 26 $\mu$m and 40 $\mu$m, respectively. The beam radius on the SESAM is 67 $\mu$m.

where $\Delta f_g$ is the FWHM gain bandwidth. The formula represents an empirical fit to results from numerical simulations.[16] Using $g \cong l + \Delta R_{ns}$ (neglecting saturable losses) and $\Delta f_g = 350$ GHz, we find $\Delta R \approx 0.015\%$. This is also very low and agrees well with the $\Delta R \times E_{sat,A}$ value retrieved from the transfer-function measurements when we assume a reasonable $F_{sat,A}$.

In conclusion, by comparing the measured transfer functions of the cw and the mode-locked laser, we can see the influence of the SESAM on the pulse-energy dynamics, but this influence is surprisingly small. The properties of the transfer functions, the measured low QML threshold, and the long pulse length all suggest that the modulation depth of the SESAM is unusually small, in a range where a sufficient accuracy of a direct measurement would be very difficult to achieve. The small modulation depth may be caused by a too high bandgap of the absorber.

### C. Er:Yb:Glass Laser at 1534 nm with 61-MHz Repetition Rate

Er:Yb:glass lasers have been passively mode locked with SESAMs as early as in 1999,[7] and wavelength-tunable pulses have been demonstrated with pulse-repetition rates as high as 25 GHz (Ref. 9). A repetition rate of 40 GHz has been demonstrated recently.[10]

The QML threshold powers of many different Er:Yb:glass lasers have been characterized by our group and were always found to be considerably lower than calculated values based on Ref. 6. To investigate this discrepancy, we examined the laser dynamics using transfer-function measurements.

Er:Yb:glass is a three-level gain material that uses ytterbium as a sensitizer to increase the pump efficiency and erbium to generate gain in the 1.5-$\mu$m region. We used a phosphate glass (QX from Kigre) with erbium and ytterbium doping densities of $7.3 \times 10^{19}$ cm$^{-3}$ and $1.8 \times 10^{21}$ cm$^{-3}$, respectively. The erbium emission and reabsorption cross sections at $\lambda_L = 1534$ nm were measured earlier in our group to be $\sigma_{em} = 0.8 \times 10^{-20}$ cm$^2$ and $\sigma_{abs} = 0.8 \times 10^{-20}$ cm$^2$, respectively. The upper-state lifetime of the erbium ions is $\tau_L = 7.9$ ms. The laser cavity is shown in Fig. 7. The 2-mm-long Brewster-angled gain medium is diode pumped at $\lambda_P = 976$ nm through one of the folding mirrors. The laser is passively mode locked with a SESAM. The parameters of the SESAM are $F_{sat,A} = (22 \pm 6)$ $\mu$J/cm$^2$, $\Delta R = (0.5 \pm 0.3)\%$, and $\Delta R_{ns} = (0.16 \pm 0.14)\%$.

The repetition rate of the laser is 61 MHz, and the pulse length is 3.0 ps. The laser generates up to 55 mW of output. The QML threshold is at 24-mW output power. The relaxation oscillations were too weak to appear in the RF spectrum, but they are expected to be at ~25 kHz for maximum output power.

#### 1. Experimental Setup for Measurement of the Transfer Function

The setup is almost the same as described above for the Nd:$YVO_4$ laser in Subsection 3.A.1. The modulation on the pump and output power is measured with a silicon and an InGaAs photodiode, respectively.

Owing to the energy transfer between the ytterbium and the erbium ions, which is not instantaneous, the transfer function of the Er:Yb:glass laser is qualitatively different from that of a simple three-level laser.

#### 2. Er:Yb System

*Differential Equations*. The Er:Yb laser can be described by a quasi-three-level system (erbium ions) that is pumped through energy transfer from ytterbium ions. Similar calculations have been done by Taccheo *et al.*[17] for cw lasers.

The rate of pumping erbium ions to the upper laser level due to energy transfer is given by

$$\left.\frac{dN_2}{dt}\right|_{Yb\to Er} = CN_1M_2,$$

where $N_1$ is the erbium ion density in the lower level, $M_2$ is the ytterbium ion density in the upper level, and $C$ is a coupling constant.

We can describe the dynamics of the ytterbium ions by

$$\frac{dM_2}{dt} = \kappa(M_1) \times \frac{P_P}{V_L h\nu_P} - \frac{M_2}{\tau_{Yb}} - CN_1M_2,$$

where $\kappa(M_1)$ describes the absorption efficiency of pump photons as a function of the population in the lower Yb level, $P_P$ is the pump power, $V_L$ is the volume of the laser mode inside the gain medium, $h\nu_P$ is the energy of the pump photons, and $\tau_{Yb}$ is the radiative lifetime of the upper ytterbium level.

Rewriting these rate equations in terms of intracavity power $P$, power gain per round trip $g$, and energy stored in the ytterbium reservoir $E_{Yb}$, we find

$$\frac{dP}{dt} = \frac{g - l - q_P(E_P)}{T_R}P,$$

$$\frac{dg}{dt} = \frac{g_0 - g}{\tau_L} - \frac{P}{E_{sat,L}}g + \frac{\nu_L}{\nu_P}C\frac{E_{Yb}}{E_{sat,L}}\left(\frac{\sigma_{em}}{\sigma_{tot}}N - \frac{E_{sat,L}}{V_L h\nu_L}g\right),$$

$$\frac{dE_{Yb}}{dt} = \kappa(E_{Yb})P_P - \frac{E_{Yb}}{\tau_{Yb}} - CE_{Yb}\left(\frac{\sigma_{em}}{\sigma_{tot}}N - \frac{E_{sat,L}}{V_L h \nu_L}g\right).$$

$N = N_1(t) + N_2(t)$ is the erbium doping density. Note that the term in large parentheses is $N_1$, the steady-state population density of the lower erbium level.

*Transfer Function*. The linearized differential equations are

$$\frac{d}{dt}\begin{pmatrix}\delta P\\ \delta g\\ \delta E\end{pmatrix} = \begin{bmatrix}\alpha & \beta & 0\\ -\gamma & -\epsilon' & m_{23}\\ 0 & m_{32} & -m_{33}\end{bmatrix}\begin{pmatrix}\delta P\\ \delta g\\ \delta E\end{pmatrix} + \kappa(E)\begin{pmatrix}0\\ 0\\ \delta P_P\end{pmatrix},$$

where the new symbols are

$$\epsilon' = \frac{1}{\tau_L} + \frac{P}{E_{sat,L}} + \frac{CE_{Yb}}{V_L h \nu_P},$$

$$m_{23} = \frac{C}{E_{sat,L}}\frac{\nu_L}{\nu_P}\left(\frac{\sigma_{em}}{\sigma_{tot}}N - \frac{E_{sat,L}}{V_L h \nu_L}g\right),$$

$$m_{32} = CE_{Yb}\frac{E_{sat,L}}{V_L h \nu_L},$$

$$m_{33} = \frac{1}{\tau_{Yb}} + C\left(\frac{\sigma_{em}}{\sigma_{tot}}N - \frac{E_{sat,L}}{V_L h \nu_L}g\right) - P_P\frac{d\kappa}{dE}(E_{Yb}).$$

Before we calculate the transfer function and the stability requirements of this system, we make the approximation $m_{32} \approx 0$. It is not obvious that this is justified, but numerical calculations comparing the approximated and the exact transfer function showed that it is valid for the laser under consideration.

With this approximation, the differential equation for $\delta E_{Yb}$ is completely decoupled. This means that the transfer function of the Er:Yb laser is the product of a three-level-laser transfer function and the transfer function of the ytterbium system:

$$\chi(\omega) = \frac{\delta P_{out}}{\delta P_P} = \frac{\delta E_{Yb}}{\delta P_P} \times \frac{\delta P_{out}}{\delta E_{Yb}} = \chi_{Yb\to Er}(\omega) \times \chi_{Er}(\omega),$$

where

$$\chi_{Yb\to Er}(\omega) = \frac{T_{oc}\beta\kappa m_{23}m_{33}}{\beta\gamma - \alpha\epsilon'}\frac{1}{1 + i\dfrac{\omega}{m_{33}}},$$

$$\chi_{Er}(\omega) = \frac{\beta\gamma - \alpha\epsilon'}{-\omega^2 + (\epsilon' - \alpha)i\omega + \beta\gamma - \alpha\epsilon'}.$$

We chose these functions so that both are dimensionless and $|\chi_{Er}(0)| = 1$. We see that $\chi_{Yb\to Er}(\omega)$ describes a low-pass filter with cut-off frequency $f_{co} = (2\pi)^{-1}m_{33}$. $\chi_{Er}(\omega)$ is the rescaled transfer function of a directly pumped erbium laser with $\epsilon$ replaced by $\epsilon'$ [see Eq. (6)].

The requirements for stability of the system are

$$\epsilon' > \alpha \quad \text{and} \quad m_{33} > 0.$$

The first requirement is a modified version of the already known QML criterion, leading to a minor change of the QML threshold, while the second requirement is automatically satisfied. The frequency of the relaxation oscillations is

$$f_{ro} = \frac{1}{2\pi}\left[\beta\gamma - \alpha\epsilon' - \frac{1}{4}(\epsilon' - \alpha)^2\right]^{1/2}.$$

*3. Results*

We have measured the transfer functions of the Er:Yb:glass laser at two different output powers of the mode-locked laser. Transfer functions of the continuous-wave laser have not been measured because the output power of the laser was too unstable, apparently due to spectral hole burning and uncontrolled hopping between the axial modes. The passively mode-locked laser is much more stable.

In a first step, the low-frequency parts of the transfer functions were analyzed. At frequencies well below the relaxation oscillation frequency, $\chi_{Er}(f)$ can be assumed constant. We use $\chi_{Yb\to Er}(f)$ in the form

$$\chi_{Yb\to Er}(f) = \frac{A}{1 + i\dfrac{f}{f_{co}}}$$

to match the transfer functions at low frequencies. We find good agreement for both powers using $f_{co} = 1.33$ kHz. We do not list the value of the parameter $A$ because the data were afterwards rescaled to meet $\chi(0) = \chi_{Yb\to Er}(0) = A = \eta_{SE}$. The experimental data and the fitted $\chi_{Yb\to Er}(f)$ (solid curve) are shown in Figs. 8(a)–8(d). We did the measurement only for two relatively low power levels (close to the QML threshold) because for higher pump powers the erbium relaxation oscillations were too strongly damped for the peak to be visible.

From $f_{co}$, we can now estimate the ytterbium-to-erbium energy-transfer coupling constant $C$. Using the relation

$$f_{co} = \frac{m_{33}}{2\pi} = \frac{1}{2\pi}\left[\frac{1}{\tau_{Yb}} + CN_1 - P_P\frac{d\kappa}{dE}(E)\right] \cong \frac{1}{2\pi}\left(\frac{1}{\tau_{Yb}} + CN_1\right),$$

where

$$N_1 = \frac{\sigma_{em}}{\sigma_{tot}}N - \frac{E_{sat,L}}{V_L h \nu_L}g,$$

we find $C \approx 2.4 \times 10^{-16}$ cm$^3$/s. By comparing $\tau_{Yb}^{-1}$ and $CN_1$, we find that the total decay rate of the upper ytterbium level is seven times higher than the spontaneous decay rate alone, assuming $\tau_{Yb}$ to be 1 ms. This indicates that the energy transfer is fairly efficient.

Now we extract $\chi_{Er}(f)$ by calculating the ratio of the measured data and the fitted low-pass transfer function. The extracted data are shown in Figs. 8(e) and 8(f). The data were fitted using the functions given in Eqs. (9) and (10) in the same way as described for the Nd:$YVO_4$ laser (Subsection 3.A.2).

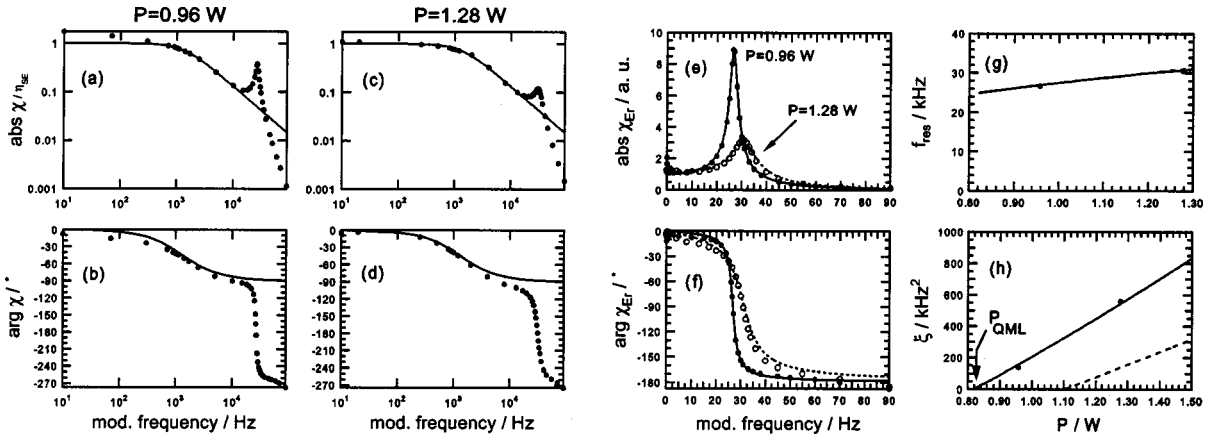


Fig. 8. (a)–(d) Modulus and phase of measured transfer functions of 61-MHz mode-locked Er:Yb:glass laser at two different intracavity powers. The low-frequency part was fitted with $\chi_{\mathrm{Yb}\rightarrow\mathrm{Er}}(f)$ (solid curves). (e), (f) By removing $\chi_{\mathrm{Yb}\rightarrow\mathrm{Er}}(f)$, we find the transfer functions $\chi_{\mathrm{Er}}(f)$ of the erbium ions alone (see text for explanation). (g), (h) $f_{\mathrm{res}}$ and $\xi$ of the measured erbium transfer functions as functions of the intracavity power. The solid curves show $\xi(P)$ and $f_{\mathrm{res}}(P)$, taking into account additional nonlinear loss in SESAM. The dashed curves [not distinguishable from the solid curve in (g)] are plotted with the additional nonlinear loss reduced to the amount expected from TPA in the SESAM (see also Fig. 9). The $\xi(P)$ corresponding to the dotted curve in Fig. 9 is not within the plotting area anymore.

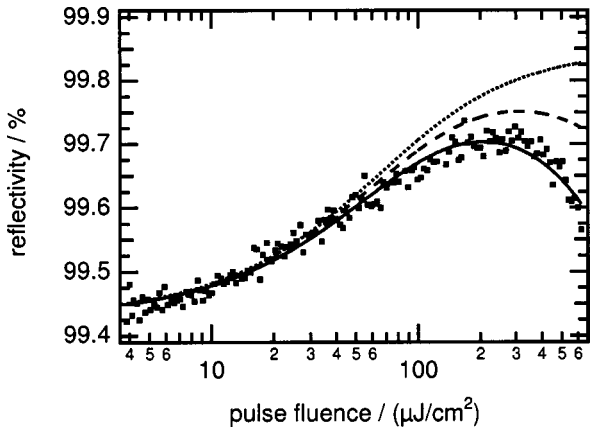


Fig. 9. Measured and fitted reflectivity curve of the SESAM used in the 61-MHz Er:Yb:glass laser. The measurement was done using 2.6-ps pulses. The rollover at high pulse fluences is clearly visible. The dotted curve shows the same reflectivity curve without the additional nonlinear loss (see the text); the dashed curve shows the reflectivity curve, including the expected amount of two-photon absorption.

Figures 8(g) and 8(h) show the parameters $f_{\mathrm{res}}$ and $\xi$ plotted as functions of the intracavity power. It is found that these data cannot be explained using laser and SESAM parameters similar to those given above. The QML threshold power is in agreement with the new QML criterion, but the damping of the relaxation oscillations (and therefore $\xi$) rises much faster than expected when increasing the pump power. Even when we allow for large deviations of the laser parameters, it is not possible to find agreement with the measured data.

The observation of fast increasing damping of the relaxation oscillations suggests the existence of an additional nonlinear loss that increases with the circulating pulse energy, because such an effect leads to a damping of deviations from the steady-state pulse energy. In the following, we assume a nonlinear loss, which increases linearly with the pulse energy with a scaling constant $a$:

$$q_{\mathrm{new}}(E_{\mathrm{P}}) = a \times E_{\mathrm{P}}. \tag{12}$$

This effect could in principle arise from two-photon absorption in the SESAM,[18] which can be used for power limiting[19] and has been shown to lower the QML threshold.[20] However, two-photon absorption in our SESAM is not expected to be strong enough to be effective for picosecond pulses. Nevertheless, the existence of this additional nonlinear loss has been verified by direct measurement of the reflectivity curve of the SESAM, which is shown in Fig. 9. For high pulse energies, the reflectivity exhibits a rollover that is well fitted with an additional term as in Eq. (12). For comparison, we have also plotted the reflectivity curves for the amount of nonlinear loss expected from two-photon absorption in our SESAM and for no additional loss at all (dashed and dotted curves in Fig. 9). An explanation for the early rollover may be photoinduced absorption in trapped carriers in localized defect states. In order to show that the additional nonlinear loss has indeed a strong influence on the relaxation oscillation dynamics, we calculated $\xi(P)$ for reduced (corresponding to the dashed curve in Fig. 9) and for no additional nonlinear loss [Fig. 8(h)]. For no additional nonlinear loss the curve even falls outside the plotting area.

With a pulse length of 2.6 ps, we measured $a = (6 \pm 2)\ \mathrm{cm}^2/\mathrm{J}/A_{\mathrm{A}}$. Because the loss is actually proportional to the pulse fluence and not the pulse energy, $a$ is inversely proportional to the beam area $A_{\mathrm{A}}$ on the SESAM.

Using Eqs. (7) and (8) (replacing $\epsilon$ with $\epsilon'$ in the formulas) we calculated $f_{\mathrm{res}}$ and $\xi$ from the laser properties. The laser and SESAM parameters were varied within their tolerance. The used values are $a = 8\ \mathrm{cm}^2/\mathrm{J}/A_{\mathrm{A}}$, $l = 5\%$, $w_{\mathrm{L}} = 29\ \mu\mathrm{m}$, $\Delta R = 0.6\%$, $F_{\mathrm{sat,A}} = 25\ \mu\mathrm{J}/\mathrm{cm}^2$, $\Delta R_{\mathrm{ns}} = 0.3\%$, and $w_{\mathrm{A}} = 61\ \mu\mathrm{m}$. Predicted and measured data are in good agreement [Figs. 8(g) and 8(h)].

### 4. Conclusions

We have derived differential equations describing the dynamics of the laser operation including the energy transfer between ytterbium and erbium ions. We showed

theoretically and experimentally that the ytterbium energy reservoir introduces a low-pass filter for perturbations of the pump power. Apart from this, the $Q$-switching dynamics of the Er:Yb:glass laser are similar to those of a directly pumped Er:glass laser.

From the measured transfer functions, we derived that the relaxation oscillations are damped more strongly than we would expect from the laser parameters. We showed that this behavior can be quantitatively explained with a nonlinear loss in the SESAM that linearly increases with the incident pulse energy. This effect has indeed been verified directly by saturation measurements on the SESAM.

By analyzing the low-pass behavior of the transfer functions, we were able to give an estimate of the coupling constant for the energy transfer between ytterbium and erbium ions.

### D. Er:Yb:Glass Laser at 1534 nm with 10-GHz Repetition Rate

We also investigated the dynamics of a miniature Er:Yb:glass laser that had been developed for the generation of 10-GHz pulse trains.[8] The QML threshold of this laser had been found to be considerably lower (factor of ~20) than theoretical predictions.

This laser (Fig. 10) has already been described in detail in Ref. 8. It uses a Brewster-angled gain medium that is diode pumped at $\lambda_P = 976$ nm through the output-coupling mirror. The laser is passively mode locked with a SESAM.

The repetition rate of the laser is 10 GHz, and the laser generates up to 20 mW of average output power. The QML threshold is at ~15 mW output power. The relaxation oscillations were too weak to appear in the RF spectrum, but they are expected to be at ~300 kHz for maximum output power.

#### 1. Results

By using the same setup as explained above in Subsection 3.C.1 for the 61-MHz Er:Yb:glass laser, we have measured the transfer functions at two different output powers of the mode-locked laser (Fig. 11). The low-frequency parts of the transfer functions were fitted with a low-pass transfer function (solid curves in Fig. 11) as explained above in Subsection 3.C.3. We find a cutoff frequency $f_{co} = 1.2$ kHz for the low pass and estimate the ytterbium–erbium energy-transfer coupling constant to be $C \approx 2.2 \times 10^{-16}$ cm$^3$/s, only slightly lower than obtained for the 61-MHz laser.

Using the method described in Subsection 3.C.3, we have tried to extract $\chi_{Er}(f)$ from the measured data.

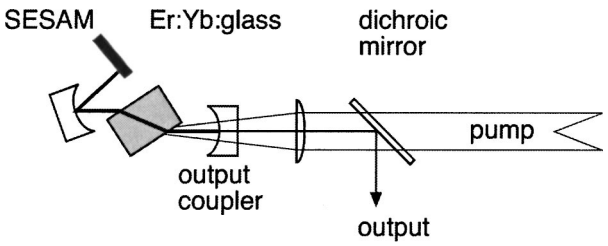


Fig. 10. Cavity of the 10-GHz Er:Yb:glass laser.

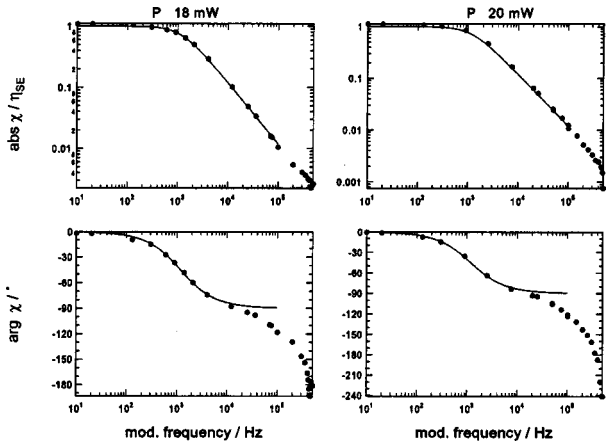


Fig. 11. Measured transfer functions of the 10-GHz mode-locked Er:Yb:glass laser. The low-frequency part was fitted with $\chi_{Yb\rightarrow Er}(f)$ (solid curves) allowing for an estimate of the energy-transfer coupling constant between the ytterbium and erbium ions.

However, the relaxation oscillation peak is too weak to reliably extract $\chi_{Er}(f)$. From the phase of $\chi(f)$, we can at least estimate $f_{res} \approx 400$ kHz, which is in agreement with our expectation. The data are not sufficient to extract the damping of the relaxation oscillations.

The small length of this laser cavity leads to a high relaxation oscillation frequency. A consequence of this is that the low pass resulting from the energy transfer causes the relaxation oscillation peak to be very weak. Therefore our method is more suitable for longer laser cavities or for lasers with direct pumping of the lasing ion.

## 4. CONCLUSIONS

We have described and demonstrated a novel type of measurement that allows us to investigate the damping of the relaxation oscillations of a passively mode-locked laser above the QML threshold. Previously, only the QML threshold itself could be measured, and no information was available on the dynamics above the QML threshold, i.e., in the usually preferred regime of operation.

We have performed this type of measurement for various lasers. For a 1-$\mu$m Nd:$YVO_4$ laser, we obtained good agreement with theoretical expectations. For a 1.3-$\mu$m Nd:YLF laser, the surprisingly low QML threshold could be explained with an unusually low modulation depth of the SESAM, which is hard to measure with other techniques.

We have also investigated the dynamics of Er:Yb:glass lasers, which are significantly modified by the energy transfer from ytterbium to erbium ions. The measurements allowed us to extract the coupling constant for the energy transfer. The damping of the relaxation oscillations could also be measured for a 61-MHz Er:Yb:glass laser and was found to be significantly stronger than expected using a simple SESAM model. However, good agreement was obtained by using measured SESAM saturation curves, which indicate the presence of a nonlinear loss, which tends to dampen the relaxation oscillations.

For a 10-GHz laser, we found that the relaxation oscillation peak was too low for the measurement of the damping of the relaxation oscillations. In conclusion, the novel method has been shown to provide useful information on the laser dynamics, the energy transfer in Er:Yb:glass, and SESAM properties.

## ACKNOWLEDGMENTS

This work was supported by the Swiss Commission for Technology and Innovation. GigaTera, Inc., has supported experiments on the Er:Yb:glass lasers. Edith Innerhofer has measured the emission and reabsorption cross sections of the used Er:Yb:glass gain material. The $Nd:YVO_4$ laser has been built by Steve Lecomte.

A. Schlatter can be reached at the address on the title page, or by telephone, 41-1-633-4094, fax, 41-1-633-1059, or e-mail, schlatter@phys.ethz.ch.

## REFERENCES

1. U. Keller, "Recent developments in compact ultrafast lasers," Nature **424**, 831–838 (2003).
2. U. Keller, D. A. B. Miller, G. D. Boyd, T. H. Chiu, J. F. Ferguson, and M. T. Asom, "Solid-state low-loss intracavity saturable absorber for Nd:YLF lasers: an antiresonant semiconductor Fabry-Perot saturable absorber," Opt. Lett. **17**, 505–507 (1992).
3. U. Keller, K. J. Weingarten, F. X. Kärtner, D. Kopf, B. Braun, I. D. Jung, R. Fluck, C. Hönninger, N. Matuschek, and J. Aus der Au, "Semiconductor saturable absorber mirrors (SESAMs) for femtosecond to nanosecond pulse generation in solid-state lasers," IEEE J. Sel. Top. Quantum Electron. **2**, 435–453 (1996).
4. U. Keller, T. H. Chiu, and J. F. Ferguson, "Self-starting and self-*Q*-switching dynamics of a passively mode-locked Nd: YLF and Nd:YAG laser," Opt. Lett. **18**, 217–219 (1993).
5. F. X. Kärtner, L. R. Brovelli, D. Kopf, M. Kamp, I. Calasso, and U. Keller, "Control of solid-state laser dynamics by semiconductor devices," Opt. Eng. **34**, 2024–2036 (1995).
6. C. Hönninger, R. Paschotta, F. Morier-Genoud, M. Moser, and U. Keller, "*Q*-switching stability limits of continuous-wave passive mode locking," J. Opt. Soc. Am. B **16**, 46–56 (1999).
7. G. J. Spühler, L. Gallmann, R. Fluck, G. Zhang, L. R. Brovelli, C. Harder, P. Laporta, and U. Keller, "Passively mode-locked diode-pumped erbium-ytterbium glass laser using a semiconductor saturable absorber mirror," Electron. Lett. **35**, 567–568 (1999).
8. L. Krainer, R. Paschotta, G. J. Spühler, I. Klimov, C. Y. Teisset, K. J. Weingarten, and U. Keller, "Tunable picosecond pulse-generating laser with a repetition rate exceeding 10 GHz," Electron. Lett. **38**, 225–227 (2002).
9. G. J. Spühler, P. S. Golding, L. Krainer, I. J. Kilburn, P. A. Crosby, M. Brownell, K. J. Weingarten, R. Paschotta, M. Haiml, R. Grange, and U. Keller, "Novel multi-wavelength source with 25-GHz channel spacing tunable over the C-band," Electron. Lett. **39**, 778–780 (2003).
10. S. C. Zeller, L. Krainer, G. J. Spühler, K. J. Weingarten, R. Paschotta, and U. Keller, "Passively mode-locked 40-GHz Er:Yb:glass laser," Appl. Phys. B **76**, 1181–1182 (2003).
11. D. Burns, M. Hetterich, A. I. Ferguson, E. Bente, M. D. Dawson, J. I. Davies, and S. W. Bland, "High-average-power (>20 W) $Nd:YVO_4$ lasers mode locked by strain-compensated saturable Bragg reflectors," J. Opt. Soc. Am. B **17**, 919–926 (2000).
12. L. Krainer, R. Paschotta, S. Lecomte, M. Moser, K. J. Weingarten, and U. Keller, "Compact $Nd:YVO_4$ lasers with pulse repetition rates up to 160 GHz," IEEE J. Quantum Electron. **38**, 1331–1338 (2002).
13. L. Fornasiero, S. Kück, T. Jensen, G. Huber, and B. H. T. Chai, "Excited state absorption and stimulated emission of $Nd^{3+}$ in crystals. Part 2. $YVO_4$, $GdVO_4$, and $Sr_5(PO_4)_3F$," Appl. Phys. B **67**, 549–553 (1998).
14. R. Fluck, G. Zhang, U. Keller, K. J. Weingarten, and M. Moser, "Diode-pumped passively mode-locked 1.3 $\mu$m $Nd:YVO_4$ and Nd:YLF lasers by use of semiconductor saturable absorbers," Opt. Lett. **21**, 1378–1380 (1996).
15. A. L. Harmer, A. Linz, and D. R. Gabbe, "Fluorescence of $Nd^{3+}$ in lithium yttrium fluoride," J. Phys. Chem. Solids **30**, 1483–1491 (1969).
16. R. Paschotta and U. Keller, "Passive mode locking with slow saturable absorbers," Appl. Phys. B **73**, 653–662 (2001).
17. S. Taccheo, P. Laporta, O. Svelto, and G. D. Geronimo, "Theoretical and experimental analysis of intensity noise in a codoped erbium-ytterbium glass laser," Appl. Phys. B **66**, 19–26 (1998).
18. E. R. Thoen, E. M. Koontz, M. Joschko, P. Langlois, T. R. Schibli, F. X. Kärtner, E. P. Ippen, and L. A. Kolodziejski, "Two-photon absorption in semiconductor saturable absorber mirrors," Appl. Phys. Lett. **74**, 3927–3929 (1999).
19. A. C. Walker, A. K. Kar, W. Ji, U. Keller, and S. D. Smith, "All-optical power limiting of $CO_2$ laser pulses using cascaded optical bistable elements," Appl. Phys. Lett. **48**, 683–685 (1986).
20. T. R. Schibli, E. R. Thoen, F. X. Kärtner, and E. P. Ippen, "Suppression of *Q*-switched mode locking and breakup into multiple pulses by inverse saturable absorption," Appl. Phys. B **70**, 41–49 (2000).